

Simulation of fracture in plain concrete modeled as a composite material

Thanh T. Bui[†] and Mario M. Attard[‡]

*School of Civil & Environmental Engineering, University of New South Wales, Sydney, Australia
(Received October 20, 2005, Accepted December 8, 2005)*

Abstract. A composite model is used to represent the heterogeneity of plain concrete consisting of coarse aggregates, mortar matrix and the mortar-aggregate interface. The composite elements of plain concrete are modeled using triangular finite element units which have six interface nodes along the sides. Fracture is captured through a constitutive single branch softening-fracture law at the interface nodes, which bounds the elastic domain inside each triangular unit. The inelastic displacement at an interface node represents the crack opening or sliding displacement and is conjugate to the internodal force. The path-dependent softening behaviour is developed within a quasi-prescribed displacement control formulation. The crack profile is restricted to the interface boundaries of the defined mesh. No re-meshing is carried out. Solutions to the rate formulation are obtained using a mathematical programming procedure in the form of a linear complementary problem. An event by event solution strategy is adopted to eliminate solutions with simultaneous formation of softening zones in symmetric problems. The composite plain concrete model is compared to experimental results for the tensile crack growth in a Brazilian test and three-point bending tests on different sized specimens. The model is also used to simulate wedge-type shear-compression failure directly under the loading platen of a Brazilian test.

Keywords: fracture; concrete; composite; cracking; Brazilian test.

1. Introduction

The safety and durability of concrete structures are significantly influenced by the fracture behaviour of concrete. There are many fracture formulations which assume concrete is a homogeneous material and provide reasonable simulations. However, such models do not include the effects of the composition of plain concrete on the macroscopic material behaviour. To better understand the physical processes involved in the fracture process, models considering the heterogeneous nature of concrete are required (Van Mier 1997, Leite, *et al.* 2004, Vonk 1991).

Since its earliest stage of development there has been intense research interest in the modeling of fracture in quasibrittle materials with the majority of the investigations limited to mode I failure. The methods proposed can be categorized into either the discrete crack methods or those based on a smeared cracking model. The difficulties in providing a numerical simulation of the fracturing process within quasibrittle materials lie with the fact that the fracturing zone is localized with softening of the load carrying capacity. Since the crack opening is discontinuous, it cannot easily be

[†] PhD Candidate, E-mail: t.bui@unsw.edu.au

[‡] Associate Professor, Corresponding Author, E-mail: m.attard@unsw.edu.au

handled by smeared cracking models.

Attard and Tin-Loi (2005) presented a discrete element representation to model plain concrete. Their formulation is based on a linear complementarity formulation (LCP) and uses a mathematical programming algorithm to obtain solutions to a nonholonomic rate formulation. A softening single branch constitutive law is used. A single event by single event strategy is adopted to trace the load-deflection response. This paper presents an algorithm for generating a heterogeneous representation of plain concrete and extends the work in Bui and Attard (2004). The formulation is based on the work of Attard and Tin-Loi (2005). Two types of tests on plain concrete are simulated and compared to experimental results. Firstly, the tensile crack growth and wedge-type shear-compression failure in a Brazilian test are studied. Secondly, results for three-point bending tests on different sized specimens are explored.

2. Composite model for concrete heterogeneity

Because of the different sizes of the constituents within the internal structure of plain concrete, the scale of the modelling detail depends on the level of simulation required and the available computational power. As discussed in Van Mier (1997) according to Zaitsev and Wittmann (1981), mechanical models for concrete can be categorised into three distinct classes of scale. At a macroscopic level, the material is considered as homogeneous and therefore do not include the composite nature of concrete. At the microscopic level, the mortar matrix is subdivided into fine aggregate and hardened cement paste with pores embedded inside. Between the macro and micro scale lies the mesoscopic level where plain concrete is regarded as a two-phase material either as small aggregates surrounded by hardened cement paste or as coarse aggregate particles embedded in a mortar matrix bonded. The mortar and aggregate particles are bonded along the interfacial zones. Van Mier (1997) believes that with the computational power available today, mesoscopic level analysis appears to be the most practicable and useful approach for evaluating the composite behaviour of concrete. Mesolevel models have successfully been used to simulate the complex fracture behaviour of concrete, as well as for investigating the influence of the concrete composition on the macroscopic properties (Sadouki and Wittmann 2000, Van Mier, *et al.* 1996).

Modelling of plain concrete on a mesoscopic scale involves firstly the generation of a coarse aggregate structure which resembles that of real concrete in terms of the distribution of aggregate size and shape. One simple method would be to position aggregate particles in a purely random fashion (Wittmann, *et al.* 1984, Schlangen and Van Mier 1992). Any particle that lies partially outside of the concrete domain or intersects other previously placed particles will be removed. This simple approach only bears a domain of low aggregate content, which in general does not resemble the real concrete. Furthermore, the many redundant dismissing steps make it a time consuming procedure. Vervuurt (1997) revised the process by dropping virtual circular particles into a mould. The horizontal position was selected randomly and the particle dropped downward until a minimum distance is obtained with the regard to the position of the previous particles. This could be done several times for a particle and the position chosen was the one lowest of all. The final grain structure is formed by omitting the smallest range particles. The final grain structure might look too coarse because of the gap among large aggregate particles. Moreover, this algorithm cannot determine exactly the aggregate content. Leite, *et al.* (2004) developed algorithm based on a stochastic-heuristic search method. If the next particle overlapped the current elements or fell

outside the specimen, a heuristic search was performed to place it in a feasible position. This method sounds long and tedious, yet produced concrete with higher aggregate content and more realistic distribution. Wittmann, *et al.* (1984) generated rounded aggregates using a morphological law developed by Beddow and Meloy (1980), as well as angular aggregates modeled using polygons with randomly chosen number of edges and corresponding angles. Schlangen and Van Mier (1992) used particle-placing method by assuming the shape of aggregate particles is spherical. For the distribution of the aggregate particles in concrete mix, a Fuller curve was used. The distribution of spherical diameters in a certain cross-section was generated using a cumulative function introduced by Walraven (1980). Wang, *et al.* (1999) also used a particle placing method. Particular attention was paid to shape and sizing of the aggregate particles. An effort was made to produce angular aggregates using polygons with prescribed elongation ratios rather than just as randomly shaped polygons.

De Schutter and Taerwe (1993) used different approach by firstly generating a mesh based on Delaunay triangulation and subsequently defining particles in each of the triangular areas, taking into account the aggregate grading curve and content.

Schlangen (1995) used the image of a real concrete section as the basis for generating a particle mesh distribution. This technique was simple but relied on the available concrete image and did not contribute to the development of mesoscopic mesh generating algorithms.

Once the particle structure has been determined the next phase is the development of the modelling mesh and the allocations of constitute properties. It is important to minimize badly shaped elements in the mesh generation process.

If the composite structure is to be analysed using a discrete method such as the lattice model, regular or random lattice mesh will be generated. Subsequently, the lattice model is superimposed on top of the generated material structure or the actual scanned section of real concrete. The beams falling inside the aggregate particles, in the matrix, or crossing the interfacial transition zone between the aggregates and the matrix, have to be assigned with the strength and stiffness of the distinctive phase, i.e., particles, matrix, and bond properties (Schlangen and Van Mier 1992, Schlangen 1993, 1995, Van Mier 1997). If the composite structure is to be analysed by continuum model, such as the well-known finite element method, a mesh for each of the three phases needs to be generated. Contrary to particle models where mesh size is smaller than particle size in the material, the mesh size might be equivalent to the smallest particle in this approach. Wang, *et al.*

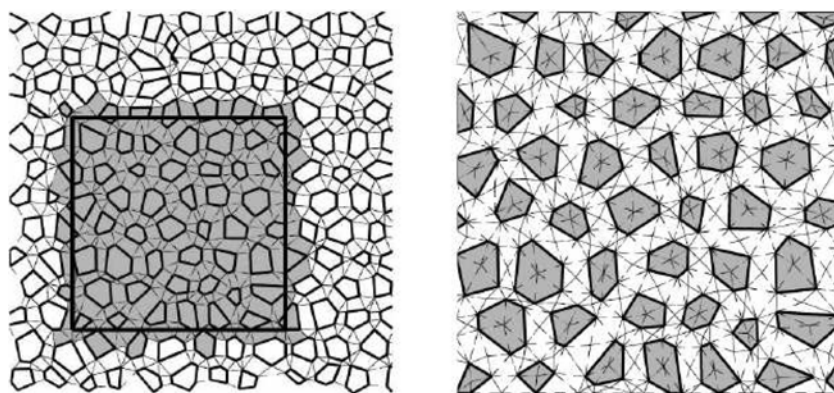


Fig. 1 Finite element mesh in particle composites after Vonk (1992)

(1999), for example, developed a mesh generation method for random aggregate structures based on the advancing front approach. It generated four-node interface elements to model interfacial zones and produces triangular meshes for the aggregate and mortar domains in which the phase boundaries are followed exactly the element boundaries.

The approach used by Vonk (1992) was to model each aggregate with a hexagonal sub-mesh consisting of six triangular elements. The hexagonal sub-mesh was embedded in a matrix. The hexagonal sub-mesh was subsequently deformed randomly to achieve a random orientation of interfaces. Fig. 1 shows the mesh structure developed by Vonk (1992). It is important to note that the method proposed by Vonk lead to rather angular aggregates, which may have some effect on the properties of the interface between aggregate and matrix. However, this method offers the benefit of producing both mesh and element properties at the same time.

The approach adopted here is to firstly generate a regular triangular mesh as in Fig. 2a. This can be done easily using any available mesh generator such as GID (the personal pre and post

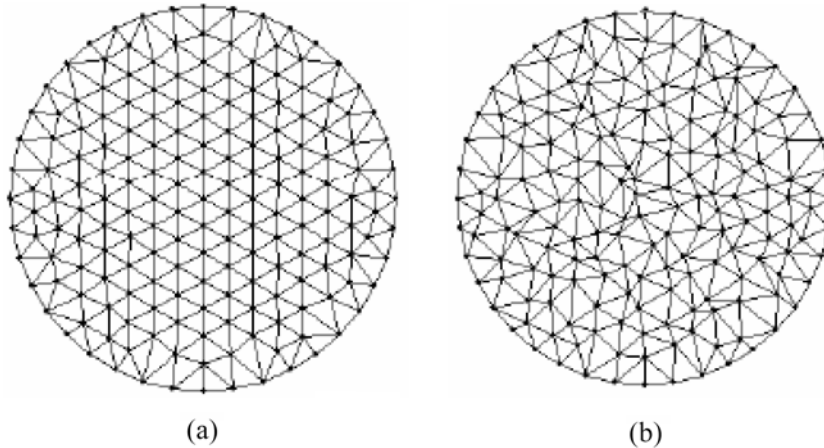


Fig. 2 Regular mesh a) and random mesh b) generated by moving nodes

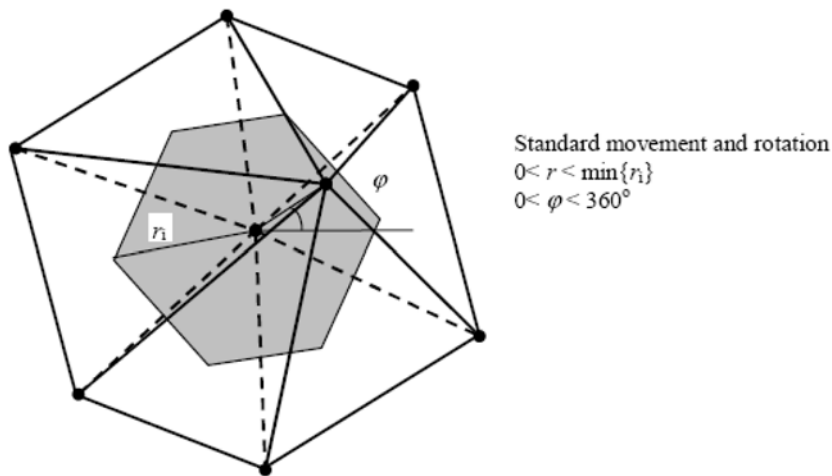


Fig. 3 Random movement of the node in its neighbouring boundary

processor, International Center for Numerical Methods in Engineering) or Easy Mesh (a two-dimensional quality mesh generator, Consortium for International Development of the University of Trieste, Italy). Secondly, each node is then randomly moved within the polygon connecting the centroid of neighbouring elements (see Fig. 3) to produce randomly orientated interfaces to the mesh structure as shown in Fig. 2b. The neighbouring elements were selected by collecting all surrounding triangle elements that have the node in common. As Fig. 3 suggested, the node in the middle had totally six elements around it, which in this case had six corresponding centroid nodes. The node then will be given a random movement and toward a random direction. All nodes, in a permuted order, will be moving to a new position.

The next stage of the meso-modelling is to define the particle allocation, i.e., the placement of the particles in the prescribed mesh. In this case, the element centre points are determined particle by particle starting with the largest ones. Initially, centre node of the first aggregate is randomly determined. The aggregate associated with this location is then formed by collecting all neighbouring triangular elements in a certain range which match approximately the aggregate size. The location of the next coarse aggregate is then randomly selected within the concrete domain. If this location allows the aggregate to lie completely within the concrete domain and does not overlap the previously placed aggregate, the location is granted. The later can be automatically satisfied by assigning minimum distance between aggregate centers. Being satisfied the given distribution for the largest aggregate size range, the second largest size range aggregate will be created in the same manner. The process continues until the range close to the smallest range. In the real process of concrete placing and compacting, the smaller particles are somehow adjusted by the settlement of the larger ones. Therefore, it is reasonable to place the larger aggregates and then smaller ones. The proposed algorithm allocates progressively the largest aggregate sizes with the more numerous smaller aggregates filling the voids between the largest aggregates. This yields a more realistic structure than a purely random procedure for all particles with different sizes. The smallest aggregate which can be modeled depends on the size of the smallest triangular element used in the mesh. The smallest mesh size can always be selected to satisfy any chosen particle ranges.

Fig. 4 shows an example of the particle generation used to represent a Brazilian test specimen. The aggregate sizes ranged from 1.2 mm for single-element aggregate to 7.2 mm. The aggregate

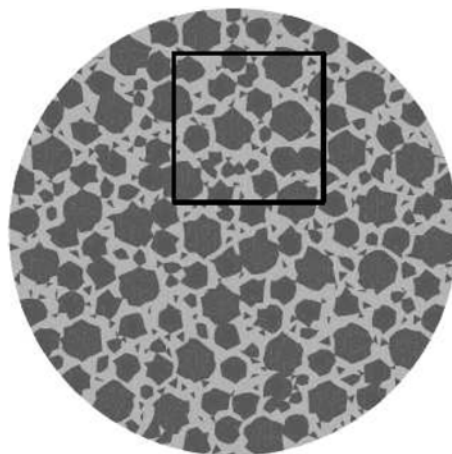


Fig. 4 The aggregate distribution in the Brazilian disk

Table 1 The coarse aggregate particle content

Aggregate Size (mm)	7.2	4.8	2.4	1.2
Number	35	69	71	238
Percentage (%)	28.54	25.19	7.27	4.47

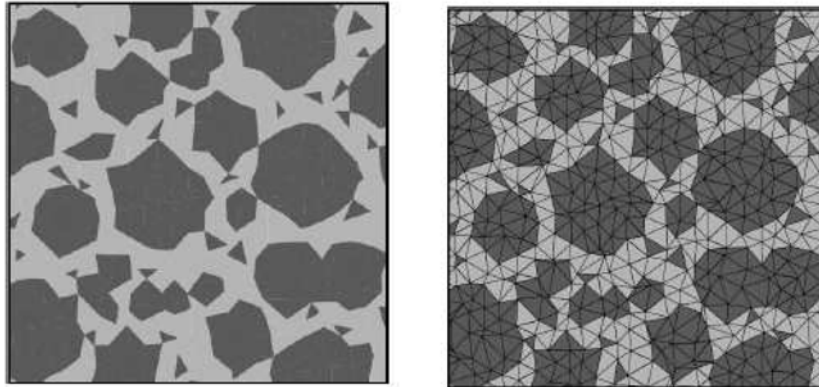


Fig. 5 A more detailed view of the mesomodelling of plain concrete taken from the mesh shown in Fig. 7

content was 65.47% of the total specimen area. Details of particle size and their content are given in Table 1.

The meshing process is completed by assigning the interface and element properties to each triangular element. Since the mesoscopic structure of concrete consists of aggregate particles embedded in a homogeneous mortar matrix, each of which is to be modeled by different elements, the two phases are treated as separate regions: the aggregate domain and the mortar matrix domain. The aggregate domain consists of the several elements grouped within the polygon representing the aggregate particle. The mortar matrix domain has a boundary formed by the edges of the polygons representing the aggregate particles. Both the aggregate and mortar matrix domains are formed by

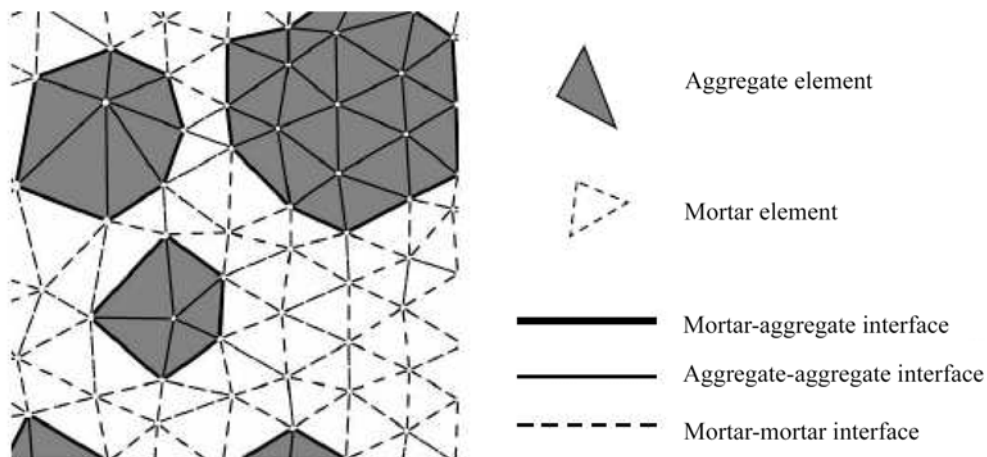


Fig. 6 The element and interface properties

triangular elements as in Fig. 6. Different shaded areas indicate different material properties assigned to various elements. Aggregate element properties are assigned to the elements falling inside the aggregate region. On the other hand, mortar properties are assigned to the elements falling inside the matrix region. In Fig. 6, aggregate elements are shaded. The aggregate-aggregate interface properties are assigned to the edges between aggregate elements, the mortar-aggregate interface properties are assigned to the edges bordering an aggregate element and a matrix element and the mortar-mortar properties are assigned to those separating matrix elements (dashed lines in Fig. 6).

The proposed generation algorithm can only match the desired aggregate content approximately. However, by reducing the mean distance between aggregate particles, the aggregate content of a generated mesh can be increased allowing for smaller aggregate particles. In this way, the desired aggregate content can be closely achieved. Furthermore, the proposed algorithm allows mesh irregularities to be controlled at the early stages by eliminating or adjusting badly shaped elements.

3. Interface elements

The numerical study presented here is based on the particle/interface type model developed by Attard and Tin-Loi (2005). The approach used a linear complementarity formulation and an enumerative mathematical programming algorithm to obtain equilibrium solutions to a nonholonomic rate formulation. The basic unit in the formulation is a triangular unit formed by assembling nine constant strain triangles and condensing out the freedoms at the vertices of the assembled unit as shown in Fig. 7. The material within the triangular unit remains linear elastic.

At the level of the interface nodes, the inelastic failure surface is a function of the normal and shear interface forces (see Fig. 7). Fig. 8 depicts the interface inelastic failure surface. It follows the classical Mohr-Coulomb type law with a tension cut-off. It is important to note that the inelastic failure surface involves interface generalized interface forces, as opposed to stresses. The constitutive inelastic failure law for the interface forces was a single branch softening law. The yield surface for a complete structure can be approximated by a piecewise linear presentation of interface

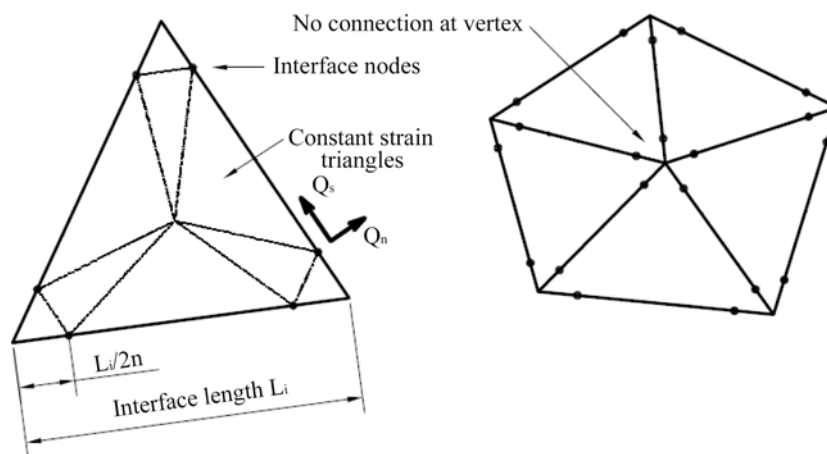


Fig. 7 Discrete triangular units

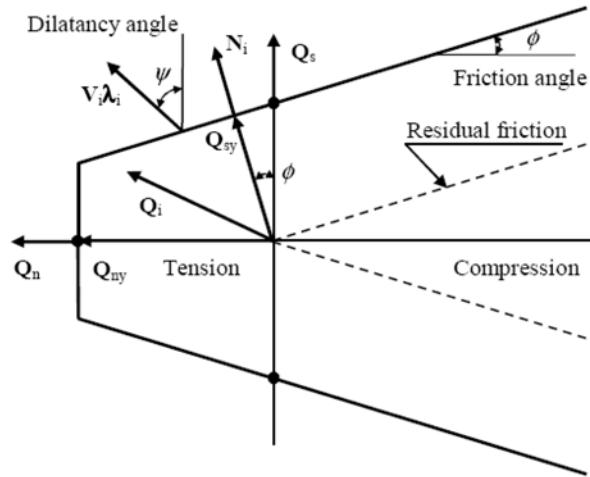


Fig. 8 Interface inelastic failure surface

yield surfaces as in classical plasticity formulation of Maier (1970). For the composite model of plain concrete the constitutive elastic and inelastic properties for the aggregate, mortar and aggregate-mortar interface are needed.

4. Analysis algorithm

In order to track the inelastic displacements such as the opening and closure of cracks, the path-dependent softening behaviour in finite incremental form needs to be solved. A more detailed description of the algorithm employed here can be found in Attard and Tin-Loi (2005). For the whole structure, the interface generalized forces are collected into the vector \mathbf{Q} . Similarly, a structure hardening and/or softening matrix \mathbf{H} , the vector of inelastic multipliers λ , the structure normality and dilatancy matrices \mathbf{N} and \mathbf{V} , respectively, and a vector \mathbf{r} containing the values for inelastic failure, are assembled for the complete structure. The evolution of the failure surface is determined by:

$$\mathbf{r} + \mathbf{H}\lambda \quad (1)$$

Inelastic failure is activated if \mathbf{Q} reaches the assembled structure inelastic failure surface. This can be ascertained by examining the projection of \mathbf{Q} ($\mathbf{N}^T\mathbf{Q}$), in all phases which then must satisfy the following condition:

$$\mathbf{N}^T\mathbf{Q} \leq \mathbf{r} + \mathbf{H}\lambda \quad (2)$$

Eq. (2) can be recast into the following form:

$$\varphi = \mathbf{N}^T\mathbf{Q} - \mathbf{r} - \mathbf{H}\lambda \leq \mathbf{0} \quad (3)$$

The following constraints must also be satisfied:

$$\lambda \geq \mathbf{0} \quad \phi^T \lambda = \mathbf{0} \quad (4)$$

Eqs. (3) and (4) can be reset in a standard Linear Complementarity Problem (LCP) format:

$$\mathbf{0} \leq \mathbf{z} = \mathbf{p} + \mathbf{M}\mathbf{x} \perp \mathbf{x} \geq \mathbf{0} \quad (5)$$

A quasi-prescribed displacement approach is also imposed such that the load vector is maintained (see Attard and Tin-Loi 2005). The problem is solved in incremental steps as a series of linear complementarity problems. At each event (next point to reach failure or critical opening or sliding displacement) a set of active multipliers is maintained and updated, with unloading inelastic failure points removed from the active set.

Unique solutions are guaranteed if the \mathbf{M} matrix is positive definite and standard algorithms such that of Lemke (1965) can be used to solve for such instances. If the \mathbf{M} matrix is not positive definite then a multiplicity of solutions could be possible indicating a bifurcation has been reached. An enumerative procedure to solve the LCP is then used if the size of the problem is not too large, as described in Bolzon, *et al.* (1997). When multiple solutions are detected, the equilibrium solution which provides the minimum increment in external work is taken as the critical solution. This approach becomes important when investigating softening and especially for interacting and/or branching cracks. For very large problems, the enumerative procedure may not achieve a solution in real time. In this case, the Lemke algorithm is adopted and a single event by event strategy is used which eliminates the occurrence of simultaneous failure/softening. For example, in a symmetric structure two symmetrically stressed points will reach failure at “exactly” the same load. A bifurcation in the load deflection response occurs because equilibrium solutions exist where both points soften, or where one of them softens and the other elastically unloads. The solution with the minimum increment in work is the latter. If simultaneous failure is disallowed the only solution possible is where one point reaches failure and softens, while the other elastically unloads. A single event by event strategy results in an asymmetric mode of failure, if one exists. Real structures with imperfections display asymmetric modes of failure (if they exist) because this involves the least work.

5. Numerical simulations

5.1. The Brazilian test

The Brazilian test was conceived independently by Carneiro and Barcellos in Brazil (Carneiro and Barcellos 1953) and by Akazawa in Japan (Akazawa 1953). A concrete cylinder is placed with its longitudinal axis horizontal between the platens of a testing machine. The load is increased until failure by tension splitting along the vertical diameter. The Brazilian test or split cylinder test has been accepted widely as an indirect measure of the tensile strength of concrete. This universal acceptance is due to the simplicity of the test and the fact that the same specimens as those used for the measurement of the compressive strength are used.

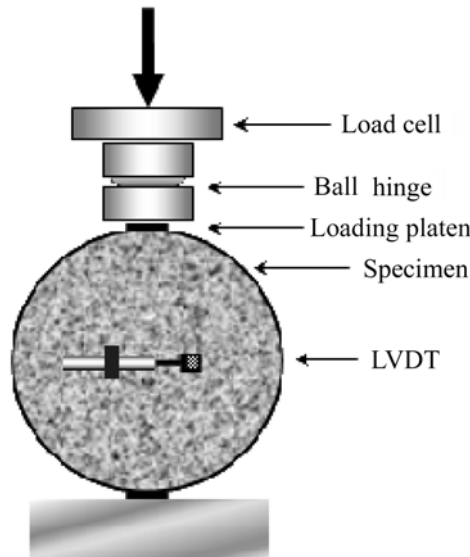


Fig. 9 A schematic illustration of a tensile splitting test

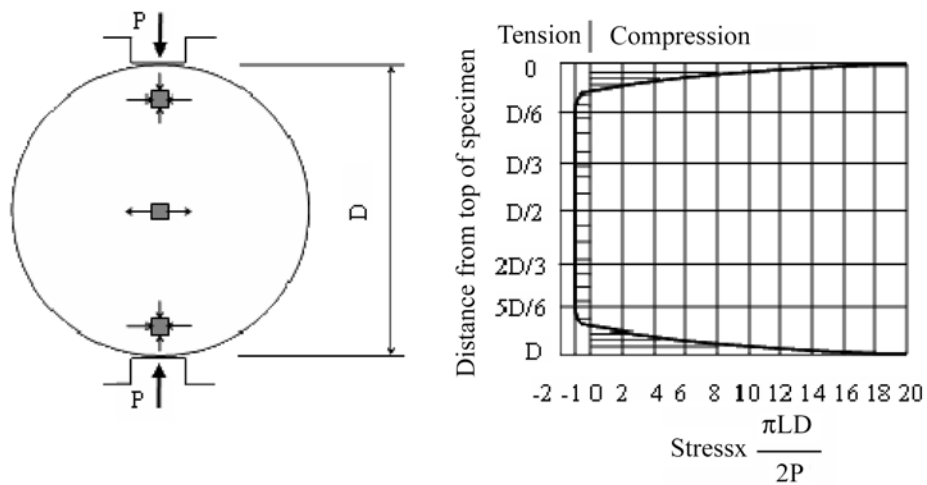


Fig. 10 Distribution of horizontal stress in Brazilian test after Wright (1995)

As stated above, a cylinder is tested on its side and subjected to compressive-load end loads, as shown schematically in Fig. 9. The elastic solution for the stress distribution within the cylinder indicates that almost constant tensile stresses act along the vertical loading axis of the specimen while triaxial compressive stresses act beneath the loading platens as indicated in Fig. 10. At the peak load, a longitudinal splitting crack propagates rapidly from the center of the cylinder towards the loading platens. During testing, sometimes secondary cracks can also propagate, producing a wedge formation near the loading platens (Lilliu, *et al.* 1999). Failure of the specimen then involves plastic slip of the wedge region under the loading platen. Slip within the wedge failure zone is affected by aggregate interlock. Hence higher ratios of cylinder splitting strength to uniaxial tensile

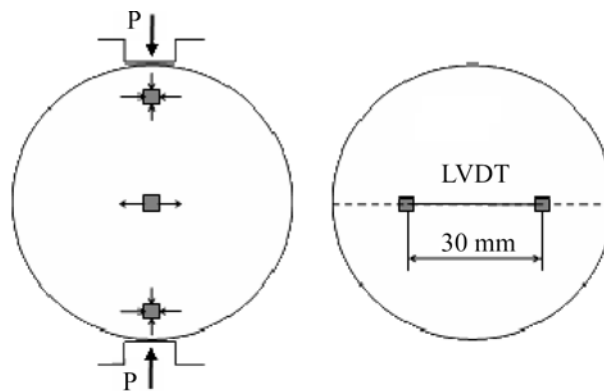


Fig. 11 Experimental setup for the Brazilian test in Lilliu and Van Mier (1999)

strength are obtained with larger aggregate sizes (Lilliu and Van Mier 1999). The fracture process zone in the Brazilian test, as discussed in Lilliu, *et al.* (1999), is influenced by many factors, including the width and type of the bearing strips beneath the loading platens.

In the experiments conducted at the M2L Laboratory, Delft Technical University (Lilliu and Van Mier 1999), the top and bottom of a cylinder specimen 75 mm in diameter was either glued to the loading platens or a 3 mm thick plywood layer was interposed between the loading platens and the specimen (see Fig. 11). For the glued case, the splitting crack did not extend completely through the diameter of the specimen. Lateral displacements beneath the loading platens were prevented by the boundary conditions producing confinement of the concrete in the zone below the loading platen. The only possibility for the splitting cracks was to propagate around the confined wedge zone below the loading platens. Two branches of the initial splitting crack were observed to propagate towards the surface of the specimen forming a wedge type zone. Secondary radial cracks also developed. For the loading case with interposed plywood sheets, a vertical splitting crack propagated the entire specimen along its diameter. The load-transverse displacement diagram showed quite ductile behaviour after the peak load. The thickness of specimens tested by Lilliu and Van Mier (1999) was 10 mm which was chosen in order to achieve an approximate plane stress state and to limit, as far as possible, any three dimensional effects. River gravel aggregates were used with a maximum size of $d_a = 8$ mm. Lilliu and Van Mier (1999) were able to perform a stable test by using a quasi-prescribed displacement control based on the relative displacement taken from an LVDT at the mid-height of the specimen (see Fig. 11). The gauge length of the midheight LVDT used to control the test was 30 mm. The test stopped when the maximum deformation of 0.35 mm was reached before complete failure of the specimen occurred.

The experimental load-displacement diagrams of Lilliu and Van Mier (1999) are shown in Figs. 12 & 13. Fig. 12 shows the results using the glued loading platen and is characterized by a first peak load at 3.942 kN and then softening to reach a minimum 3.437 kN. After that it hardens to a second peak load of 4.946 kN. The two peaks corresponded to the principle and secondary fracture processes, respectively. Transverse forces could still be transmitted through the surfaces of the splitting crack, once it had propagated. The magnitude of such forces increased with the roughness of the crack surfaces. During this stress transferred via “aggregate interlock”, the crack opened while the load increased slowly. At this stage, the load-displacement diagram showed a long plateau until the second peak, which was related to plastic slip of the wedge prior to failure. When the

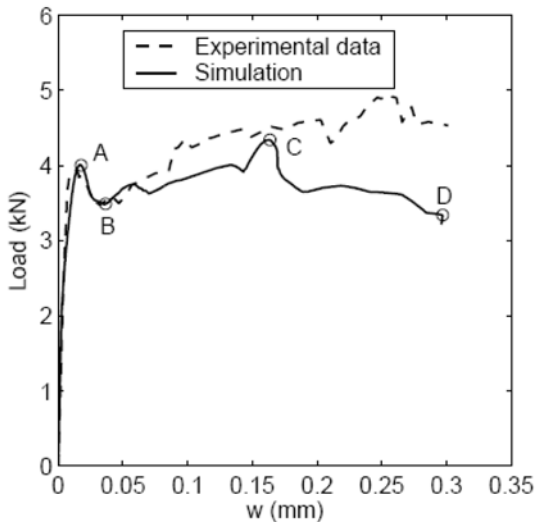


Fig. 12 The load-displacement curve from experiment and simulation (glued loading platen)

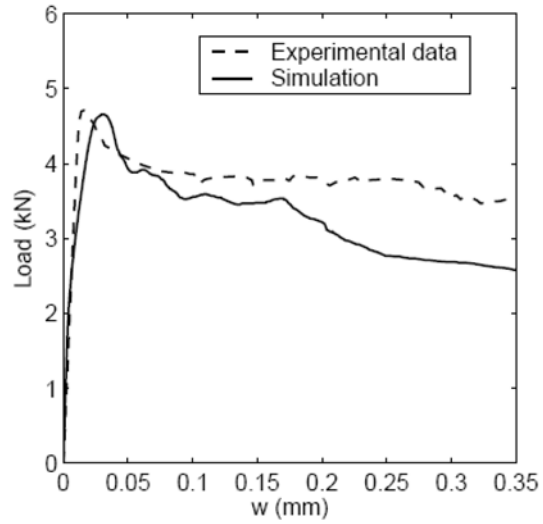


Fig. 13 The load-displacement curve from experiment and simulation (plywood loading platen)

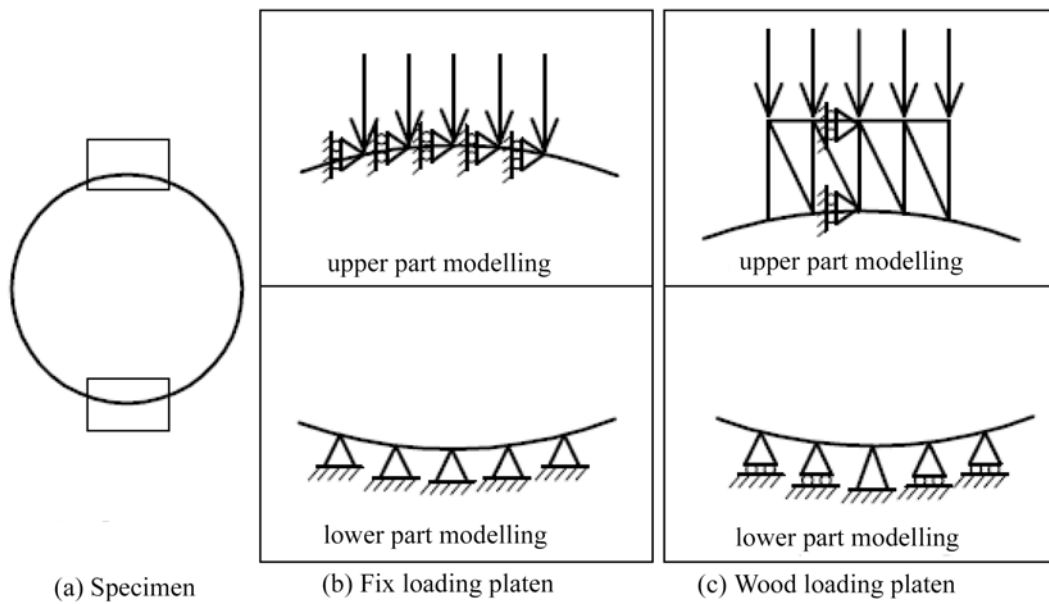


Fig. 14 Boundary condition modeling

specimen was tested with a plywood plate between the loading platen, the load vs. longitudinal displacement experienced only one peak at 4.748 kN. After that, the load decreased slowly and the vertical crack opened completely to the specimen boundary.

The composite mesh used to model the Brazilian test is shown in Fig. 15. The loading of the specimen was simulated by imposing distributed vertical loads at the top of the specimen. To simulate the glued fixed loading platen, loaded vertical rollers were used as shown in Fig. 14. To

Table 2 Interface material properties

Phase	Mortar-mortar	Mortar-aggregate
Comp. strength (MPa)	46	23
Mode I – fracture energy (Nmm/mm ²)	0.019	0.003
Tensile strength (MPa)	1.65	1.32
Mode II – fracture energy (Nmm/mm ²)	3	1.5
Friction angle (radian)	0.3	0.3
Dilatancy angle (radian)	0	0

simulate the plywood loading platen, a rigid block was modeled with the central upper and lower midspan nodes prevented from moving sideward (see Fig. 14). Vertical loading was applied through the rigid block. The lower part of the specimen was assigned with either horizontal rollers or pinned supports as shown in Fig. 14. The interface cohesion between the rigid block and the specimen was set to a very small quantity. The friction angle of the interface between the rigid block and the concrete was set to zero.

Table 2 lists the interface material properties adopted in the simulation of the test specimen of Lilliu and Van Mier (1999). The aggregate type quoted by Lilliu and Van Mier (1999) was river gravel. Since they did not list the fracture properties of the constitute elements of their concrete, several material properties had to be estimated. The interface properties were taken from a number of studies that were summarized extensively in the monograph by Van Mier (1997). The Young's modulus for the aggregate and the mortar were taken as 70,000 N/mm² and 25,000N/mm², respectively.

Some of the simulation results for the test with the glued loading platen are shown in Figs. 12, 15 and 16. Fig. 12 shows a comparison of the experimental load versus the relative deflection results (the relative deflection was measured at the mid-height of the specimen over a gauge length of 30 mm as depicted in Fig. 11) with that of the simulation. The simulation load-displacement diagram displayed a first peak as in the experiments, followed by a local minimum (event B) and a second peak load. At the first peak load (event A), a vertical macro-crack developed (see Fig. 15). The crack did not propagate through the entire specimen but stopped beneath the loading platen. At this

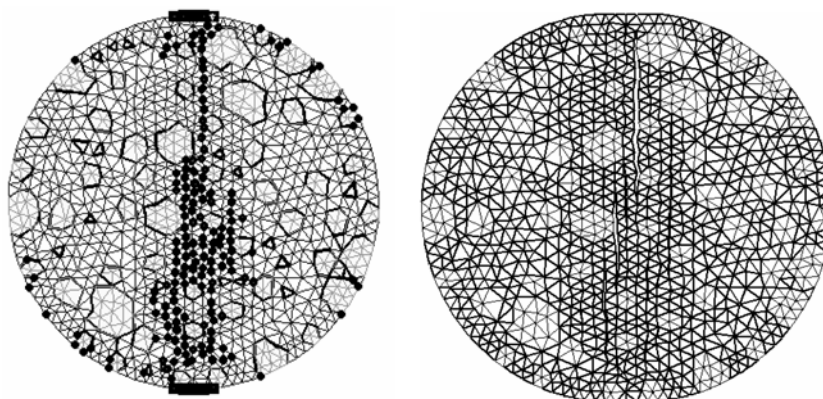


Fig. 15 The crack path and deformed shape at the first peak. The black circles correspond to points activating the tension failure surface

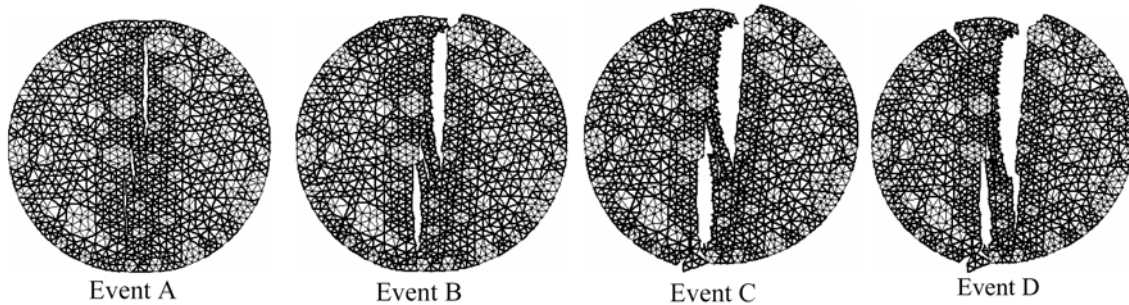


Fig. 16 The deformed specimen with glued platen in different events

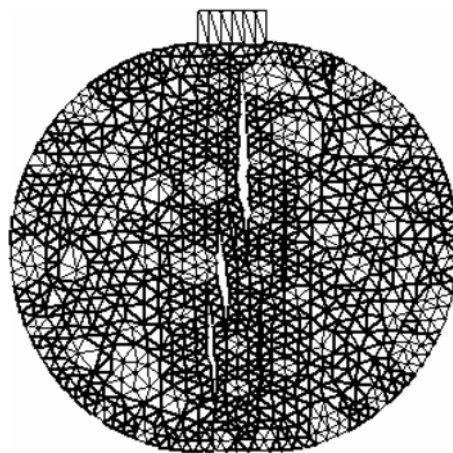


Fig. 17 The deformed specimen with a plywood platen after peak load

stage only micro-cracks were present between the loading platen. Fig. 16 shows the crack path at various stages along the post-peak path (note the crack opening displacement is not drawn to scale but has been exaggerated). At the second peak load (event C) a radical crack begins at the surface of the specimen and propagates inwards as the load decreases. After a while, a second radical crack forms and the load level is maintained at nearly constant level. A splitting crack also propagates from the surface further into the top of the specimen. More micro-cracks form at the top and the bottom of the specimen, near the loading platens. These micro-cracks start to coalesce, producing the formation of wedges. However, when the simulation is continued, complete failure of the specimen is not obtained. The two radical cracks continue to propagate and new radical cracks form. This limitation of the simulation maybe because there is no compression cap in the failure surface and hence complete compression failure cannot be captured.

For the boundary condition with a sheet of plywood between the loading platen and the specimen, the splitting crack started from the middle and coalesced longitudinally along its diameter. A low friction coefficient was given to the interfaces between the loading platen and the specimen which allowed lateral displacements at the contact interface. Two or more short cracks developed parallel to each other (see Fig. 17). In this case, the cracks extended through the entire diameter of the specimen. During this process the crack opened while the load decreased slowly. During this stage, the load-displacement diagram showed a long plateau (as in Fig. 13). The crack profile showed a similar response to the observed cracks in the test carried out by Lilliu and Mier (1999).

5.2. Three-point bending tests

One essential material parameter of the cohesive crack model is the mode I fracture energy G_F . Because of several difficulties involved in using the direct uniaxial tension test, a simpler test method, the three-point bending test, is routinely used to measure the mode I fracture energy. The three-point bending test is also used to determine the governing parameters for the size effect model of Bažant, *et al.* (1991) and the two-parameter model of Jenq and Shah (1985). The test procedures have been standardised in accordance with RILEM (RILEM 1985). The three-point bending test is also used to measure the flexure bending tensile strength of many materials.

In a three-point bending test, a beam specimen with a central notch is vertically loaded at midspan by a stiff testing apparatus. In most cases, a closed-loop servo controlled testing machine is used to ensure a stable test. The beam is supported close to its ends by roller bearings. The test is then performed by monotonically increasing the displacement until the specimen breaks into two halves. During testing, the displacement at the centre of the beam and the corresponding load is registered.

The simulation here concerns the notched three-point bending beam tests of Jenq and Shah (1985). Three different sized beams were used in Jenq and Shah (1985) with a view to checking the validity of several concrete fracture models in the literature for size effects. All beams were geometrically similar and were designated as large (C1L1), medium (C1M2) or small (C1S3). All

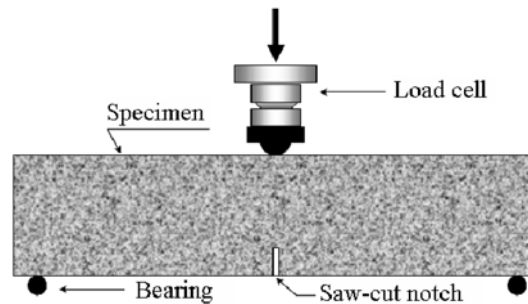


Fig. 18 Illustration of a three-point bending test

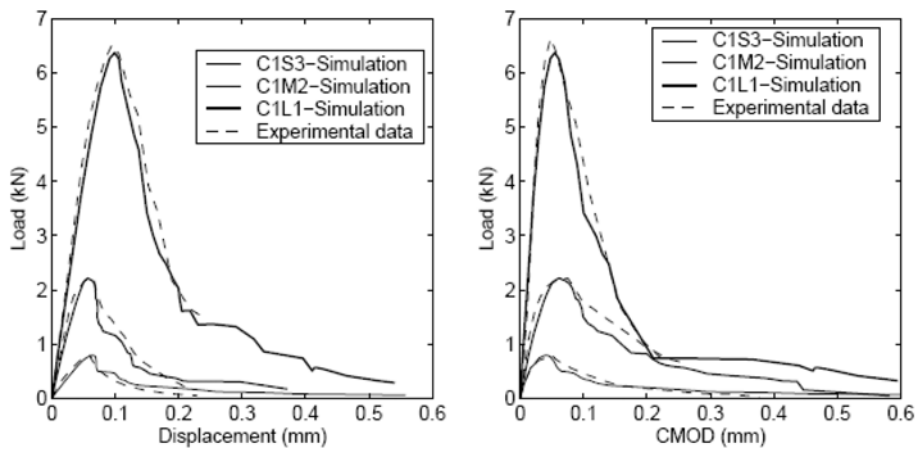


Fig. 19 The load vs. deflection and CMOD from experiment and simulation

Table 3 Specimen dimensions for the three-point bending test

Type	Large	Medium	Small
Span (mm)	914	609	305
Height (mm)	229	152	76
Thickness (mm)	85.7	57.2	28.6
Notch depth (mm)	76.2	50.8	22.3

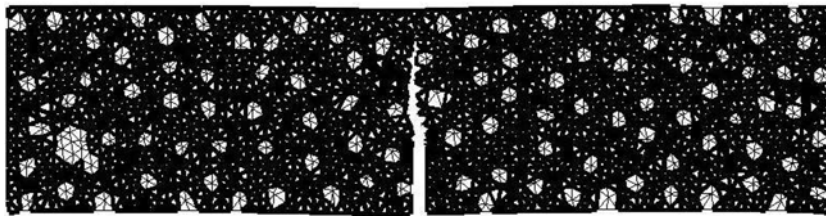


Fig. 20 The deformed shape after load step 231 for the medium-size beam

beams had an initial notch depth which was equal to one-third of their depth. The tests were carried out in a servocontrolled closed-loop testing machine. All beams were tested so as to maintain a constant rate of increase of crack mouth opening displacement (CMOD). The mesh showing the aggregate layout was partially showed in Fig. 20. For all three beams the same mesh size was generated, i.e., 8 mm, which produced maximum aggregate size of approximate 16mm. Lots of single aggregates were made in the domain left by larger size aggregates. The aggregate content was roughly 45% for all simulated specimens.

Here we used the interface parameters used in the previous Brazilian simulation (see Table 4) but the mode I fracture energy had been modified accordingly to the test carried out by Jenq and Shah (1985). The mode I fracture energy for the mortar-aggregate interface was taken as 0.103 N/mm, 0.09 N/mm, and 0.06615 N/mm for the large, medium and small specimens, respectively.

The load vs. midspan deflection of the small, medium and large specimens are given in Fig. 19. The displacement given was measured at the load point. The simulation is compared to a representative result in each experimental test. Fig. 19 shows the corresponding load versus CMOD curves. The CMOD is taken equal to the difference between the horizontal displacements of simulation corner nodes at the mouth of the notch. The simulation shows excellent agreement with the experimental results for the three different sized specimens with the one set of material properties. The crack trajectory tended to go around the coarse aggregates as expected in normal strength concrete.

6. Conclusions

A finite element formulation which models plain concrete as a composite consisting of aggregate particles, the mortar matrix and the interfaces has been presented. The finite element formulation consists of a mesh of triangular units with nodes along the interface sides as proposed in Attard and Tin-Loi (2005). The inelastic process is captured through constitutive laws for the normal and shear forces at the interface nodes. A single branch softening law is used. The cracking and inelastic

sliding is limited to the interfaces of the mesh. Material properties are assigned for the aggregate, mortar and aggregate-mortar interfaces. A new approach for generating the aggregate particle as well as the mesh was adopted. The algorithm is capable of producing both mesh and aggregate, which has the advantage of ruling out the badlyshaped triangular elements. A Mohr-Coulomb failure surface with a tension cut-off has been adopted. The path dependent softening behaviour was solved using an incremental non-holonomic rate formulation using a mathematical programming algorithm.

The numerical simulations of the Brazilian test and three point bend test have been presented. The heterogeneous character of concrete has been modeled with various elements representing aggregates, mortar and the aggregate-mortar interface. The solution strategy was based on the particle/interface model developed by Attard and Tin-Loi (2005). Material properties for the constituents of concrete had to be estimated. The history of the crack path development and the load versus displacement/crack mouth opening displacement response matched the experimental results well.

The fracture process in a Brazilian test when glued as well as plywood loading platens are used had been simulated and compared to experimental results by Lilliu and Van Mier (1999). The fracture mechanism involved both mode I fracture along the vertical axis of loading and shear-compression wedge type failure beneath the loading platen as observed in glued loading. The post-peak path demonstrated a slightly stiffening load path because of the fact that the tensile crack was hampered by the shear-compression region under the bearing pad. Whereas, when no longitudinal restraint was introduced, which mimicked the plywood platen simulation, the crack went straight to the boundary.

Current work is aimed at applying the same methodology to the solution of problems with unknown, possibly interacting crack itineraries and including other constituents, i.e., steel fibre. Modelling concrete failure under compression is also a feasible choice.

Acknowledgements

This study is partially supported financially by the Australian Research Council and the International Postgraduate Research Scholarship scheme funded by the Australian Department of Education, Science and Training.

References

- Akazawa, T. (1953), "Tension test method for concrete", Int. Assoc. of Testing and Research Laboratories for Materials and Structures, Bull. No. 16.
- Attard, M.M. and Tin-Loi, L. (2005), "Numerical simulation of quasibrittle fracture in concrete", *Eng. Frac. Mech.*, **72**(3), February, 387-411.
- Bazant, Z. P., Kazemi, M. T., Hasegawa, T., Mazars, J. (1991), "Size effect in Brazilian split-cylinder tests: measurements and fracture analysis", *ACI Materials J.*, **88**(3), 325-332.
- Beddow, J. K., and Meloy, T. (1980), "Testing and characterization of powders and fine particles", London; Heyden.
- Bolzon, G., Maier, G. and Tin-Loi, F. (1997), "On multiplicity of solutions in quasi-brittle fracture computations", *Computational Mechanics*, **19**, 511-516.
- Bui, T. T. and Attard, M. M. (2004), "Numerical simulation of the Brazilian test", in *ACMSM 18, Development in Mechanics of Structures and Materials*, Deeks, A. J. and Hao, H. Eds., Balkema, Perth, Australia, 197-203.
- Carneiro, F. L. L. B., and Barcellos, A. (1953), "Concrete tensile strength", Int. Assoc. of Testing and Res. Laboratories for Materials and Structures. Bull. No. 13.

- De Schutter, G and Taerwe, L. (1993), "Random particle model for concrete based on Delaunay triangulation", *Material Structures*, **26**, 67-73.
- Jenq, Y. S. and Shah, S. P. (1985), "Two parameter fracture model for concrete", *J. Eng. Mech. ASCE*, **111**, 1227-1241.
- Leite, J. P. B., Slowik, V., and Mihashi, H. (2004), "Computer simulation of fracture processes of concrete using mesolevel models of lattice structures", *Cement Conc. Res.*, **34**, 1025-1033.
- Lemke, C. E. (1965), "Bimatrix equilibrium points and mathematical programming", *Management Science*, **11**, 681-689.
- Lilliu, G and Van Mier, J. G. M. (1999), "Analysis of crack growth in the Brazilian test", *Construction Materials: Theory and Application*, H. W. Reinhardt Birthday Commemorate Volume, 123-137.
- Lilliu, G, Van Mier, J. G. M, and Van Vliet, M. R. A. (1999), "Analysis of crack growth of the Brazilian test: experiments and lattice analysis", *Proceedings ICM8*, **1**, 273-278.
- Maier, G (1970), "A matrix structural theory of piecewise-linear elastoplasticity with interacting yield planes", *Meccanica*, **5**, 54-66.
- RILEM Draft Recommendation (1985), "50-FMC Committee fracture mechanics", *Materials and Structures*, **18** (106), 285-290.
- Roelfstra, P. E., Sadouki, H., and Wittmann, F. H. (1985), "Numerical concrete", *Material Structures (RILEM)*, **18**, 327.
- Sadouki, H. and Wittmann, F. H. (2000), "Modeling of micro cracking induced by drying and endogenous shrinkage in cement composites", *International Conference on Advanced Materials, Their Processes and Applications*, Munich, Germany, Werkstoffwoche-Partnerschaft GbR, Frankfurt, Germany.
- Schlangen, E. (1993), "Experimental and numerical analysis of fracture process in concrete", *Heron*, **38**.
- Schlangen, E. (1995), "Computational aspects of fracture simulations with lattice models", in *Proceedings FraMCoS-2*, Wittmann, F. Eds., AEDIFICATIO Publishers, Freiburg, 913.
- Schlangen, E. and Van Mier, J. G. M. (1992), "Simple lattice model for numerical simulation of fracture of concrete materials and structures", *Material Structures*, **25**, 534-542.
- Schlangen, E. and Van Mier, J. G. M. (1992), "Experimental and numerical analysis of micromechanisms of fracture of cement-based composites", *Cement Conc. Compo.*, **14**, 105.
- Van Mier, J. G. M., Schlangen, E., and Vervuurt, A. (1996), "Tensile cracking in concrete and sandstone: Part 2. Effect of boundary rotations", *Material Constructions*, **29**, 87-96.
- Van Mier, J. G. M. (1997), *Fracture Processes of Concrete: Assessment of Material Parameters for Fracture Models*, CRC Press, Boca Raton.
- Vervuurt, A. (1997), "Interface Fracture in Concrete", PhD thesis, Delft University of Technology, The Netherlands.
- Vonk, R. A. (1992), "Softening of Concrete Loaded in Compression", PhD thesis, Eindhoven University of Technology, The Netherlands.
- Walraven, J. C. (1980), "Aggregate interlock: a theoretical and experimental analysis", PhD thesis, Delft University of Technology, The Netherlands.
- Wang, Z. M., Kwan, A. K. H., and Chan, H. C. (1999), "Mesoscopic study of concrete I: Generation of random aggregate structure and finite element mes", *Comput. Struct.*, **70**, 533-544.
- Wittmann, F. H., Roelfstra, P. E., and Sadouki, H. (1984), "Simulation and analysis of composite structures", *Material Science and Engineering*, 239-248.
- Wright, P. J. F. (1955), "Comments on an indirect tensile test on concrete cylinders", *Mag. Conc. Res.*, **7**(20), 87-96.
- Zaitsev, Y. B. and Wittmann, F. H. (1981), "Simulation of crack propagation and failure of concrete", *Materials Constructions*, **14**, 357-365.